Dynamic Molecular Structure of Plant Biomass-derived Black Carbon (Biochar)

- Supporting Information -

Marco Keiluweit[†], *Peter S. Nico*[‡], *Mark G. Johnson*[§], *and Markus Kleber*[†,*]

[†] Oregon State University
[‡] Lawrence Berkeley National Laboratory, Earth Science Division
[§] U.S. Environmental Protection Agency

Journal: Environmental Science & Technology

Submitted: 12-23-2009

Table of Contents (SI)

Tables and Figures (SI)

Experimental Section (SI)

(i) Char Production

Commercially available Ponderosa pine shavings (*Pinus ponderosa*) were purchased through GEM shavings LLC in Auburn, WA. Tall Fescue straw (*Festuca arundinacea*) was collected at the Oregon State University Hyslop Field Research Laboratory in Corvallis, OR. An automated plant-material grinder was used to obtain particle sizes of less than 1.5 mm for all materials. The ground plant materials were then air-dried at 40˚C for 48 hours to establish similar moisture contents. Leaving a head-space of about 100 mL, 280 g of ground plant material were placed in a heat-resistant Inconel 601 crucible (1500 mL; Metal Technology Inc., Albany, OR) and covered with a tight fitting Inconel lid to create oxygen-limiting conditions during the charring process. The plant biomass in the crucibles occupied 90% of the available space, leaving 150 mL headspace filled with air. Given that the O_2 content of air is approximately 20%, the charring process occurred in the presence of 30 mL O_2. With an average density of 1.309 g/L at 25˚C and a total biomass of 280 g, the O_2 availability amounts to ~8×10^{-5} g O_2 per g biomass.

The filled crucibles were placed in a 550 Series Fisher Scientific Isotemp muffle furnace (Fisher Scientific, Pittsburgh, PA) preheated to 100, 200, 300, 400, 500, 600 or 700˚C and charred at ambient pressure and atmosphere. The reported temperatures represent oven temperatures during preparation. The actual reaction temperature may differ from these values due to endothermic reactions during dehydration and exothermic reactions during pyrolysis. After charring for 1 hour, the closed crucible was immediately moved to a desiccator and allowed to cool. After weighing, the charred residue was transferred to airtight containers and stored in the dark. Char samples were milled to pass a <0.25 μm sieve (60 mesh) prior to further analyses. The char samples are hereafter referred to as WX00 (wood) and GX00 (grass) with "X"

indicating the final charring temperature (100-700˚C). For comparison, fresh plant material (W000 and G000) receiving the same treatment was included in some analyses.

(ii) Char Characterization

All chars were subjected to proximate analysis according to the American Society for Testing and Materials (ASTM) D1762-84 method (*1*). Essentially, in this analysis the char is heated in a covered crucible to 950 °C and held at this temperature for 6 min. The measured weight loss is defined as volatile matter (VM), and the residual solid is fixed C. Subsequently, the carbonized char is heated in an open crucible to 750 °C and held at this temperature for 6 h. The material that remains in the crucible is defined to be ash. The reported char yield is the dry mass of char produced divided by the dry mass of the precursor (grass or wood) loaded into the crucible. The interested reader finds more information on proximate analyses and typical values for volatile matter and fixed carbon yields in Antal and Gronli (*2*).

(iii) BET-N_2 surface area

Specific surface areas of all char samples were obtained with N_2-adsorption measurements at liquid nitrogen temperature (77 K) using an NOVA 2200e surface area analyzer (Quantachrome Instrument Corp., Boynton Beach, FL) and ultra high purity (99.999%) gaseous nitrogen (Polar Cryogenics, Portland, OR). Degassing of the samples was performed in sample tubes at 60˚C under continuous N_2 gas flow for ~12h. The adequacy of degassing times was validated using the method described in the ASTM D4820-97 for black carbon N_2 adsorption measurements (*3*). Nitrogen adsorption was measured for a relative pressure range of 0.01-0.03 and specific surface areas were obtained from the most linear portion of the isotherm using a minimum of 10 data points. SAs were calculated based on the Brunauer-Emmett-Teller (BET)

equation after Brunauer et al. (*4*) with a molecular surface area for N_2 of 0.162 nm^2. All N_2 measurements were performed in triplicate (N = 3).

(iv) Fourier transform infrared spectroscopy

Attenuated total reflectance Fourier transform infrared (ATR FT-IR) spectroscopy was performed using a Thermo Nicolet Nexus 470 FT-IR 6700 spectrophotometer equipped with a smart endurance single-bounce diamond ATR accessory (Thermo Fisher Scientific, Waltham, MA). Complete temperature series of grass and wood chars were scanned in the mid-infrared region from 4000 to 400 cm^{-1}. For each sample, 128 co-added spectra were recorded at a resolution of 2 cm^{-1} and processed using the OMNIC 2.1 software. A detailed account of the peak assignments can be found in the Supporting Information (SI) (Table S-1).

(v) X-ray diffraction

Approximately 1.5 g of ground sample was back loaded into a 2.5 cm diameter circular cavity holder and run on a PANanalytical X'Pert Pro Instrument using Co-Kα radiation at 40 kV and 40 mA. Diffraction patterns were recorded by step scanning from 10-60° 2θ, with the sample spinning at 2 revolutions per second. For easier display, scans were subjected to a standardized background correction and noise reduction procedure using the X'pert High Score plus software and PlotIT 3.1.

(vi) Near-edge X-ray absorption fine structure (NEXAFS) spectroscopy

Detailed operation principles of STXM/NEXAFS are published elsewhere (*5*-*7*) and will be described here only briefly.

Ground char particles were distributed on silicon nitride membranes with a thickness of 50 nm. Stacks of STXM images were acquired at the carbon K-edge (280-320 eV) for particles which allowed transmission of the X-ray beam. NEXAFS spectra were extracted from each stack

105 for specific regions of the image. The fine structure in the C 1s NEXAFS region spans the energy
106 range of 283 to 290 eV; above 290 eV transitions tend to be very broad and overlap with the
107 absorption edge(s). Potential radiation damage of the char samples (*8*) was minimized by
108 consistently avoiding dwell times of less than 1.5 ms.

109 A minimum of three distinct particles with mean diameter of less than 20 μm were
110 selected for each type of char. To avoid spectral distortion, spectra were extracted from particles
111 or areas of the particles with an optical density of less than 1.5. The extracted spectra were
112 averaged over multiple regions and, if possible, the entire particle. The spectra for each particle
113 were normalized to unity at the 310 eV position. Within temperature treatments, spectra were
114 nearly congruent, allowing us to obtain a representative spectrum for each char sample by
115 averaging over the spectra of the three particles. Peak assignment was based upon the references
116 listed in Table S-2.
117

Results and Discussion (SI)

(i) 1s-π* exciton phenomenon (NEXAFS)

If electronic excitation of an ion in a crystal is considered, the excitation corresponds to the removal of an electron from one orbital of a molecule and its elevation to an orbital of higher energy, the excited state of the molecule can be envisaged as the coexistence of an electron and a hole. Extensive highly conjugated sp^2-bonded carbon domains such as graphene permit the electron and the hole to migrate. This mobile excitation is referred to as an exciton (*9, 10*).

1s-σ* exciton signals were found in NEXAFS spectra of graphite (*11-14*), carbon nanotubes (*15-17*) and carbonaceous particulate matter (*5, 18, 19*).

(ii) Fourier transform infrared spectroscopy

The evolution of FT-IR spectra of wood and grass chars as a function of charring temperature is shown in Fig. 1. No FT-IR detectable chemical changes occur as plant material is heated to 100 and 200˚C. More noteworthy changes occur at 300˚C, particularly for grass char. After heating to 300˚C, there were stronger C=O and C=C stretching vibrations at 1700 and 1600 cm^{-1} indicating the formation of ketones, anhydrides, esters, and carboxylic C as well as aromatic components (*20, 21*). At the same time the absorbance of the dominant C-O stretch at 1030 cm^{-1} associated with cellulose, hemicellulose, and lignin slightly decreased.

Heating to 400˚C results in more substantial chemical transformations. Bands due to hydrogen bonded O-H stretching (3200-3500 cm^{-1}) of water molecules loose intensity. Absorption of the aliphatic C-H stretching (2935 and 2885 cm^{-1}) decreases slightly but sustains a strong presence indicative of heat-resistant aliphatic structures. Greater aromatic C=C stretching vibrations (1600 cm^{-1}) become the dominant feature for both wood and grass chars. Further

141 evidence for aromatic C is provided by the appearance of three bands between 885 and 750 cm^{-1}
142 (out-of-plane deformations of aromatic C-H (*21, 22*)). The signals near 815 and 750 cm^{-1} may
143 indicate O-substitution of quinone and furan-like structures (*23*). Specifically, the presence of
144 ring C-H stretch bands at 3200 cm^{-1} suggests five-membered N/O-heterocycles such as furan and
145 pyrrole (*22*).

146 The intensity of bands reflecting undecomposed cellulosic and ligneous C decline (most
147 obvious at 1030 cm^{-1}) at 400˚C. Conversely, both wood and char spectra show evidence for
148 lignin- and cellulose-derived transformation products. Ligneous products are reflected in more
149 prominent peaks at 1440 (C=O stretching of ketones) and 1375 cm^{-1} (O-H bending of phenols).
150 Cellulose-derived products in wood are suggested by bands at 1185 and 1270 cm^{-1},
151 corresponding to C-O stretching of pyranone rings and guaiacyl monomers, respectively. Signals
152 at 1180-1030 cm^{-1} in grass chars may arise from the C-H deformation of cellulose-derived
153 substituted aromatics (*24*).

154 Between 500 and 700˚C, all features related to water, oxygenated substituents, aliphatic
155 C, and the aromatic C=C stretch progressively decline. Two exceptions from this trend involving
156 aromatic components are absorption by C-H stretching (3050 cm^{-1}) and C-H out-of-plane
157 vibrations (885-750 cm^{-1}). An increase of intensity at 885-752 relative to 1650-1500 cm^{-1}
158 indicates a larger degree of condensation (*21*). Heating from 400 to 700˚C progressively
159 increases this ratio, confirming that smaller (substituted) aromatic units condense into larger
160 sheets. At 700˚C, any residual C functionalities diminish and grass and wood char spectra
161 become very similar. Both resemble closely FT-IR spectra of pure graphite (as displayed, e.g., in
162 (*25*).

163 The fact that the baseline of both wood and char is progressively shifted upward with
164 increasing temperature is a common phenomenon in spectra of carbonized materials (*26*). As a
165 result of increasing diffuse absorption of the sample, the upward shift is assigned to low-energy
166 electron excitations of condensed aromatic structures (*25*).
167 To summarize, FT-IR spectra show (i) dehydration of cellulosic and ligneous
168 components starting at 300˚C, (ii) a strong presence of (heterocyclic) aromatic C and
169 lignin/cellulose-derived transformation products at 400˚C, and (iii) an increasing degree of
170 condensation at charring temperatures of 500˚C and beyond.
171

Environmental Implications (SI)

(i) Persistence in the Environment

At the center of an ongoing debate over the extent to which chars and other forms of BC are able to persist in soils and sediments is the so-called "paradox of refractory-labile BC" (*27*). It refers to a lack of mechanistic knowledge to explain large observed differences in residence time between seemingly refractory forms and such that appear to be more dynamic. Our investigation has revealed structural and chemical discontinuities which make it plain that the persistence of black in the environment does not only depend on environmental drivers, but also and likely to a much greater extent on its particular chemistry and physical structure. We believe that investigations based on the suggested categories and individual char phases may prove particularly useful for studies that intend to rationalize observed variations in the chars' resistance to abiotic and biotic degradation (or "aging") (*28-30*).

We find our assessment supported by a study in which chars produced at different temperature were subjected to an oxidative ("aging") treatment. Trompowsky et al. (*31*) then quantified acid and alkali extractable components. Alkali extraction yield was greatest for chars produced at intermediate temperatures (450˚C), consistent with the behavior of a amorphous char as it points to components that are readily degraded and extracted from the char matrix. For chars produced at temperatures 500 and 550˚C, lower yields were attributed to the higher degree of condensation. Accordingly, these materials fall into the composite char category. It is conceivable that in such chars, single molecules of an otherwise readily extractable phase are 'trapped' by a second increasingly condensed and/or crystalline phase – a suggestion to this end has been published previously by Almendros et al. (*32*). At lower temperatures (300-400˚C), with chars most likely belonging to the transition char category, low extractability may result

194 from the microcrystalline structure of native cellulose which hinders the release of more heat-
195 altered, thus smaller molecules.

196 **(ii) Chars as Environmental Sorbents**

197 A clear distinction between the categories of chars and their various phases entering
198 soils and sediments will aid the more accurate description of the sorption behavior of organic
199 contaminants.

200 Different types of char have different BC-water distribution coefficients (K_{BC}) (*33*).
201 This variation among different chars is thought to be due to differences in SA and pore size
202 distributions, both of which are characteristic of specific char category.

203 The two-phase model proposed by Chun et al. (*34*) and Chen et al. (*20*) divides chars
204 into a non-condensed partition (absorption) medium and carbonized phases that are viewed as a
205 sorbent surface, but is indifferent toward the molecular properties of the non-condensed phase.
206 Our results show that mobile, non-condensed components may comprise both crystalline (i.e.,
207 native cellulose) and heat-altered amorphous components (i.e., lignin residues, paraffins, and
208 small (poly)aromatic units). It is to be expected that these phases show dissimilar sorptive
209 behavior, calling for a more detailed consideration of chemical composition and the physical
210 state of individual char components.

211 We anticipate that recognition of chemical and physical variation within char will also
212 facilitate the investigation of mechanisms controlling the sorption of organic compounds to chars
213 on a molecular level. Some experimental studies have utilized small graphene units as surrogates
214 of chars (*35, 36*). These authors proposed Van der Waals forces and π-π electron donor-acceptor
215 interactions with planar graphene sheets as the dominant retention mechanisms. Adsorption by
216 chars comparable to turbostratic chars may also proceed through a pore-filling mechanism (*37*).

Yet both mechanisms are intimately linked to the presence of condensed components. It is clear that the presence of non-condensed phases or varying quantities of turbostratic crystallites in any given char would affect the effectiveness of such mechanisms. Thus, these insights gained on the sorptive mechanisms remain specific to single categories of char. Because chars derived from materials other than wood (e.g., grass) show less distinguished crystalline character even at the same charring conditions, it remains to be shown to which extent the results from existing adsorption studies can be generalized

(iii) Quantification in Environmental Systems

The determination of the influence on sorption of char and its persistence in soil and sediments, is complicated by difficulties in quantifying char in such environments. Despite substantial progress, different techniques yield widely varying BC "contents" for soils and sediments (*38*). The authors of this study conclude that all quantification methods are selective, e.g., for amorphous wood char or more condensed wood chars. We suggest to consider that the quantification protocols tested might be selective for one or more char categories as delineated in this paper.

232

TABLE S-1: Assignment of characteristic vibrations to individual peaks in wood and grass char ATR FT-IR spectra.

Wavenumber [cm^{-1}]	Characteristic vibrations	Functionality
3665	'free' O-H stretching	alcoholic and phenolic -OH, not hydrogen bonded (*39*) (*40*)
3200-3500	O-H stretching	water, H-bonded hydroxyl (-OH) groups (*39*) (*40*)
3200	C-H stetching	5-membered N/O-heterocyclic C (e.g., furans and pyrroles) (*22*)
3050	C-H stretching	substituted aromatic C (*22*)
2935	asymmetric C-H stretching	aliphatic CH_x (*41*)
2885	symmetric C-H stretching	aliphatic CH_x (*41*)
1740-1700	C=O stretching	mainly carboxyl (*20*); traces of aldehydes, ketones and esters (*42*) (*43*)
1600	C=C stretching	aromatic components (*20*) (*44, 45*)
	C=O stretching	C=O of conjugated ketons and quinones (*20*) (*44, 45*)
1510	C=C stretching	aromatic skeletal vibrations, indicative of lignin (*44, 45*) (*46*)
1440	C=C stretching	aromatic C, indicative of lignin, appears when bound to unsaturated group (*44, 45*) (*46*)
	α-C-H_2 bending	aliphatic -CH_2 deformations (*40*), associated with lignin and carbohydrates (*47*)
1375	O-H bending	in plane bending of phenolic -OH (*48*), related to ligneous syringyl units (*46*)
	α-C-H_3 bending	aliphatic -CH_3 deformations (*20*) (*44, 45*)
1270-1250	C-O stretching	C-O-C groups and aryl ethers (*40*) (*20*); phenolic C-O indicative of guaiacyl units associated with lignin (*46*) (*49*)
1185-1160	(asymmetric) "	C-O-C ester groups in cellulose and hemicellulose (*24*) (*47*)
1110	(symmetric) "	C-O-C stretching vibrations in cellulose and hemicellulose [j]; aliphatic -OH (*39*)
1030	"	acid derivatives, aliphatic C-O-C, and -OH representative of oxygenated functional groups of cellulose and hemicellulose (*43*) (*47*); methoxy groups of lignins (*49*)
1200-1000	C-H deformation	vibrations typical for substituted aromatics (*24*)
885, 815, 750	C-H bending	aromatic CH out-of-plane deformation (*44, 45*); less substituted rings appear at lower wavenumbers (*39*)

233

233

TABLE S-2: Peak assignments for C forms obtained from C (1s) NEXAFS

Photon energy [eV]	Transition	C form	Functionality
284.3	1s-π*	C=C	quinone (*50*)
285.3	1s-π*	C=C	unsaturated/aromatic (*51*); graphitic (*11, 12*)
286.4	1s-π*	C=O	ketone, carbonyl substituted aromatic (*18, 52, 53*)
287.1 - 287.3	1s-3p/σ*	C-H	aliphatic (*52, 54, 55*)
	1s-π*	C-OH	phenol -OH (*55*); aliphatic -OH (*56*)
		C-OR	O-substituted aromatic C (*50*) (*8*)
288.6	1s-π*	C=O	carboxyl (*52*); aldehyde (*55*)
289.2 - 289.3	1s-3p/σ*	C-O	alcohols (*52*) (*54*)
		C-O	secondary alcohols in polysaccharides, hemicellulose and cellulose, propyl side chains and methoxyl carbons of lignin (*8*)
291.2 - 291.6	1s-σ* exciton	C-C	extensive conjugated aromatic sheets (*13, 14, 57, 58*)
292 - 295	1s-σ*	C-C	aromatic (*12, 55*); long-range order (*59*)

234

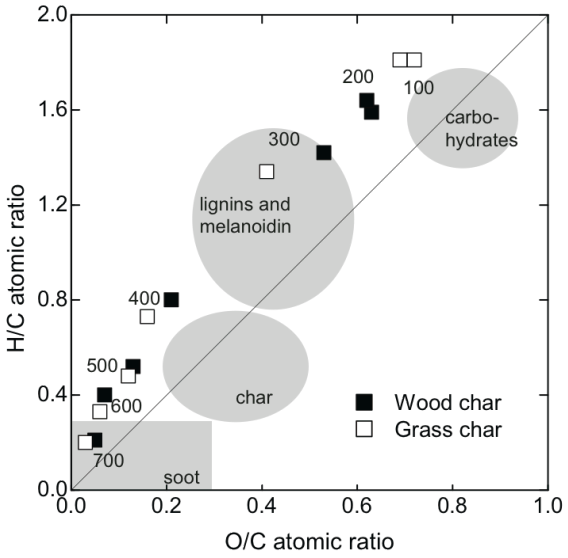

Figure S-1: Van Krevelen plot of elemental ratios for wood and grass chars. Continuous line denotes the direction of dehydration reactions due the loss of H and O (2:1 ratio in H_2O) and grey shadings highlight approximate elemental ratios of unaltered biomacromolecules (lignin, melanoidin, and carbohydrates) and black carbon materials (char and soot) following Hammes et al. (*60*).

240
241 **Literature cited (SI)**

242 (1) ASTM, D1762-84 Standard Test Method for Chemical Analysis of Wood Charcoal.
243 Conshohocken, PA, 2007.

244 (2) Antal, M.; Gronli, M., The art, science, and technology of charcoal production. Ind. Eng.
245 Chem. Res. **2003,** 42(8), 1619-1640.

246 (3) ASTM, D4820-97 Standard Test Methods for Carbon Black—Surface Area by Multipoint
247 B.E.T. Nitrogen Adsorption. Conshohocken, PA, 1998.

248 (4) Brunauer, S.; Emmett, P. H.; Teller, E., Adsorption of gases in multimolecular layers. J. Am.
249 Chem. Soc. **1938,** 60, 309-319.

250 (5) Braun, A., Carbon speciation in airborne particulate matter with C (1s) NEXAFS
251 spectroscopy. J. Environ. Monit. **2005,** 7(11), 1059-1065.

252 (6) Kilcoyne, A. L. D.; Tyliszczak, T.; Steele, W. F.; Fakra, S.; Hitchcock, P.; Franck, K.,
253 Interferometer-controlled scanning transmission X-ray microscopes at the advanced light source.
254 J. Synchrotron Rad. **2003,** 10, 125-136.

255 (7) Warwick, T.; Ade, H.; Kilcoyne, D.; Kritscher, M.; Tylisczcak, T.; Fakra, S.; Hitchcock, A.;
256 Hitchcock, P.; Padmore, H., A new bend-magnet beamline for scanning transmission X-ray
257 microscopy at the Advanced Light Source. J. Synchrotron Rad. **2002,** 9, 254-257.

258 (8) Cody, G.; Brandes, J.; Jacobsen, C.; Wirick, S., Soft X-ray induced chemical modification of
259 polysaccharides in vascular plant cell walls. J. Electron Spectrosc. Relat. Phenom. **2009,** 170(1-
260 3), 57-64.

261 (9) Atkins, P. W.; de Paula, J., Physical Chemistry. 8th ed.; Oxford University Press: Oxford,
262 2006.

263 (10) Liang, W. Y., Excitons. Phys. Edu. **1970,** 5, 226-228.

264 (11) Ahuja, R.; Bruhwiler, P.; Wills, J.; Johansson, B.; Martensson, N.; Eriksson, O., Theoretical
265 and experimental study of the graphite 1s x-ray absorption edges. Phys Rev B **1996,** 54(20),
266 14396-14404.

267 (12) Batson, P., Carbon-1s near-edge-absorption fine-structure in graphite. Phys. Rev. A **1993,**
268 48(4), 2608-2610.

269 (13) Bruhwiler, P.; Maxwell, A.; Puglia, C.; Nilsson, A.; Anderson, S.; Martensson, N., Pi-
270 asterisk and sigma-asterisk excitations in C-1s absorption of graphite. Phys. Rev. Lett. **1995,**
271 74(4), 614-617.

272 (14) Coffman, F.; Cao, R.; Pianetta, P.; Kapoor, S.; Kelly, M.; Terminello, L., Near-edge x-ray
273 absorption of carbon materials for determining bond hybridization in mixed sp2/sp3 bonded
274 materials. Appl. Phys. Lett. **1996,** 69(4), 568-570.

275 (15) Abbas, M.; Wu, Z.; Zhong, J.; Ibrahim, K.; Fiori, A.; Orlanducci, S.; Sessa, V.; Terranova,
276 M.; Davoli, I., X-ray absorption and photoelectron spectroscopy studies on graphite and single-
277 walled carbon nanotubes: Oxygen effect. Appl. Phys. Lett. **2005,** 87(5), 051923.

(16) Banerjee, S.; Hemraj-Benny, T.; Balasubramanian, M.; Fischer, D. A.; Misewich, J. A.; Wong, S. S., Surface chemistry and structure of purified, ozonized, multiwalled carbon nanotubes probed by NEXAFS and vibrational spectroscopies. ChemPhysChem **2004,** 5(9), 1416-1422.

(17) Pong, W.; Yueh, C.; Chang, Y.; Tsai, M.; Chang, Y.; Chen, Y.; Lee, J.; Wei, S.; Wen, C.; Chen, L.; Chen, K.; Lin, I.; Cheng, H., X-ray absorption studies of carbon-related materials. J. Synchrotron Rad. **2001,** 8, 145-149.

(18) Braun, A.; Mun, B. S.; Huggins, F. E.; Huffman, G. P., Carbon speciation of diesel exhaust and urban particulate matter NIST standard reference materials with C(1s) NEXAFS spectroscopy. Environ. Sci. Technol. **2007,** 41(1), 173-178.

(19) Hopkins, R. J.; Tivanski, A. V.; Marten, B. D.; Gilles, M. K., Chemical bonding and structure of black carbon reference materials and individual carbonaceous atmospheric aerosols. J. Aerosol Sci. **2007,** 38(6), 573-591.

(20) Chen, B.; Zhou, D.; Zhu, L., Transitional adsorption and partition of nonpolar and polar aromatic contaminants by biochars of pine needles with different pyrolytic temperatures. Environ. Sci. Technol. **2008,** 42(14), 5137-5143.

(21) Guo, Y.; Bustin, R. M., FTIR spectroscopy and reflectance of modern charcoals and fungal decayed woods: implications for studies of inertinite in coals. Int. J. Coal Geol. **1998,** 37(1-2), 29-53.

(22) Lin-Vien, D.; Colthup, N. B.; Fateley, W. G.; Grassell, J. G., The handbook of infrared and raman characteristic frequencies of organic molecules. Academic Press, Inc.: San Diego, CA, 1991.

(23) van der Marel, H. M.; Beutelspacher, H., Atlas of infrared spectroscopy of clay minerals and their admixtures. Elsevier Scientific Pub.: New York, 1976.

(24) Pastorova, I.; Botto, R. E.; Arisz, P.; Boon, J., Cellulose char structure - a combined analytical PY-GC-MS, FTIR, and NMR-study. Carbohydr. Res. **1994,** 262(1), 27-47.

(25) Mochidzuki, K.; Soutric, F.; Tadokoro, K.; Antal, M. J.; Toth, M.; Zelei, B.; Varhegyi, G., Electrical and physical properties of carbonized charcoals. Ind. Eng. Chem. Res. **2003,** 42(21), 5140-5151.

(26) Friel, J. J. M., S.; Follweiler, D. M., Electron optical and IR spectroscopic investigation of coal carbonization. In Coal and coal products: Analytical characterization techniques, Fuller, E. L., Ed. American Chemical Society: Washington, DC, 1982; p 294.

(27) Czimczik, C. I.; Masiello, C. A., Controls on black carbon storage in soils. Global Biogeochem. Cycles **2007,** 21(3), GB3005, doi:10.1029/2006GB002798.

(28) Baldock, J. A.; Smernik, R. J., Chemical composition and bioavailability of thermally altered Pinus resinosa (Red Pine) wood. Org. Geochem. **2002,** 33(9), 1093-1109.

(29) Hamer, U.; Marschner, B.; Brodowski, S.; Amelung, W., Interactive priming of black carbon and glucose mineralisation. Org. Geochem. **2004,** 35(7), 823-830.

(30) Cheng, C.; Lehmann, J.; Thies, J. E.; Burton, S. D.; Engelhard, M. H., Oxidation of black carbon by biotic and abiotic processes. Org. Geochem. **2006,** 37(11), 1477-1488.

(31) Trompowsky, P. M.; Benites, V. D.; Madari, B. E.; Pimenta, A. S.; Hockaday, W. C.; Hatcher, P. G., Characterization of humic like substances obtained by chemical oxidation of eucalyptus charcoal. Org. Geochem. **2005,** 36(11), 1480-1489.

(32) Almendros, G.; Knicker, H.; Gonzalez-Vila, F. J., Rearrangement of carbon and nitrogen forms in peat after progressive thermal oxidation as determined by solid-state C-13 and N-15-NMR spectroscopy. Org. Geochem. **2003,** 34(11), 1559-1568.

(33) Koelmans, A. A.; Jonker, M. T. O.; Cornelissen, G.; Bucheli, T. D.; Van Noort, P. C. M.; Gustafsson, O., Black carbon: The reverse of its dark side. Chemosphere **2006,** 63(3), 365-377.

(34) Chun, Y.; Sheng, G.; Chiou, C.; Xing, B., Compositions and sorptive properties of crop residue-derived chars. Environ. Sci. Technol. **2004,** 38(17), 4649-4655.

(35) Sander, M.; Pignatello, J., Characterization of charcoal adsorption sites for aromatic compounds: Insights drawn from single-solute and Bi-solute competitive experiments. Environ. Sci. Technol. **2005,** 39(6), 1606-1615.

(36) Zhu, D.; Pignatello, J., Characterization of aromatic compound sorptive interactions with black carbon (charcoal) assisted by graphite as a model. Environ. Sci. Technol. **2005,** 39(7), 2033-2041.

(37) Nguyen, T. H.; Cho, H.-H.; Poster, D. L.; Ball, W. P., Evidence for a pore-filling mechanism in the adsorption of aromatic hydrocarbons to a natural wood char. Environ. Sci. Technol. **2007,** 41(4), 1212-1217.

(38) Hammes, K.; Schmidt, M. W. I.; Smernik, R. J.; Currie, L. A.; Ball, W. P.; Nguyen, T. H.; Louchouarn, P.; Houel, S.; Gustafsson, Ö.; Elmquist, M., Comparison of quantification methods to measure fire-derived (black/elemental) carbon in soils and sediments using reference materials from soil, water, sediment and the atmosphere. Global Biogeochem. Cycles **2007,** 21(3), GB3016, doi:10.1029/2006GB002914.

(39) Pretsch, E.; Bühlmann, P.; Badertscher, M., Structure Determination of Organic Compounds. Springer-Verlag: Berlin, 2009.

(40) Smith, D. M.; Chughtai, A. R., The surface-structure and reactivity of black carbon. Colloid Surface A **1995,** 105(1), 47-77.

(41) Chen, B.; Johnson, E.; Chefetz, B.; Zhu, L.; Xing, B., Sorption of polar and nonpolar aromatic organic contaminants by plant cuticular materials: Role of polarity and accessibility. Environ. Sci. Technol. **2005,** 39(16), 6138-6146.

(42) Koch, A.; Krzton, A.; Finqueneisel, G.; Heintz, O.; Weber, J.; Zimny, T., A study of carbonaceous char oxidation in air by semi-quantitative FTIR spectroscopy. Fuel **1998,** 77(6), 563-569.

(43) Pradhan, B.; Sandle, N., Effect of different oxidizing agent treatments on the surface properties of activated carbons. Carbon **1999,** 37(8), 1323-1332.

(44) Bustin, R.; Guo, Y., Abrupt changes (jumps) in reflectance values and chemical compositions of artificial charcoals and inertinite in coals. Int. J. Coal Geol. **1999,** 38(3-4), 237-260.

(45) Haberhauer, G.; Rafferty, B.; Strebl, F.; Gerzabek, M., Comparison of the composition of forest soil litter derived from three different sites at various decompositional stages using FTIR spectroscopy. Geoderma **1998,** 83(3-4), 331-342.

(46) López-Pasquali, C. E.; Herrera, H., Pyrolysis of lignin and IR analysis of residues. Thermochim. Acta **1997,** 293(1-2), 39-46.

(47) Labbe, N.; Harper, D.; Rials, T., Chemical structure of wood charcoal by infrared spectroscopy and multivariate analysis. J. Agric. Food Chem. **2006,** 54(10), 3492-3497.

(48) Lehmann, J.; Liang, B. Q.; Solomon, D. H.; Lerotic, M.; Luizao, F.; Kinyangi, J.; Schafer, T.; Wirick, S.; Jacobsen, C., Near-edge X-ray absorption fine structure (NEXAFS) spectroscopy for mapping nano-scale distribution of organic carbon forms in soil: Application to black carbon particles. Global Biogeochem. Cycles **2005,** 19(1), GB1013, doi:10.1029/2004GB002435.

(49) Liu, Q.; Wang, S.; Zheng, Y.; Luo, Z.; Cen, K., Mechanism study of wood lignin pyrolysis by using TG-FTIR analysis. J. Anal. Appl. Pyrolysis **2008,** 82(1), 170-177.

(50) Francis, J. T.; Hitchcock, A. P., Inner-shell spectroscopy of para-benzoquinone, hydroquinone, and phenol - distinguishing quinoid and benzenoid structures. J. Phys. Chem. **1992,** 96(16), 6598-6610.

(51) Urquhart, S. G.; Ade, H.; Rafailovich, M.; Sokolov, J. S.; Zhang, Y., Chemical and vibronic effects in the high-resolution near-edge X-ray absorption fine structure spectra of polystyrene isotopomers. Chem. Phys. Lett. **2000,** 322(5), 412-418.

(52) Cody, G. D.; Ade, H.; Wirick, S.; Mitchell, G. D.; Davis, A., Determination of chemical-structural changes in vitrinite accompanying luminescence alteration using C-NEXAFS analysis. Org. Geochem. **1998,** 28(7-8), 441-455.

(53) Hitchcock, A. P.; Urquhart, S. G.; Rightor, E. G., Inner-shell spectroscopy of benzaldehyde, terephthaladehyde, ethyl benzoate, terephthaloyl chloride, and phosgene - models for core excitation for poly(ethylene-terephthalate). J. Phys. Chem. **1992,** 96(22), 8736-8750.

(54) Brandes, J. A.; Lee, C.; Wakeham, S.; Peterson, M.; Jacobson, C.; Wirick, S.; Cody, G., Examining marine particulate organic matter at sub-micron scales using scanning transmission X-ray microscopy and carbon X-ray absorption near edge structure spectroscopy. Mar. Chem. **2004,** 92(1-4), 107-121.

(55) Cody, G.; Botto, R.; Ade, H.; Behal, S.; Disko, M.; al., e., Inner-shell spectroscopy and imaging of a subbituminous coal: In-situ analysis of organic and inorganic microstructure using C (1s)-, Ca (2p)-, and Cl (2s)-NEXAFS. Energy Fuels **1995,** 9, 525-533.

(56) Myneni, S. C. B. In Applications of synchrotron radiation in low-temperature geochemistry and environmental sciences, Reviews in Mineralogy and Geochemistry, Jan 1, 2002; Fenter, P. A.; Rivers, M. L.; Sturchio, N. C.; Sutton, S. R., Eds. Mineralogical Society of America: 2002; pp 485-579.

(57) Brandes, J. A.; Cody, G. D.; Rumble, D.; Haberstroh, P.; Wirick, S.; Gelinas, Y., Carbon K-edge XANES spectromicroscopy of natural graphite. Carbon **2008,** 46(11), 1424-1434.

(58) di Stasio, S.; Braun, A., Comparative NEXAFS study on soot obtained from an ethylene/air flame, a diesel engine, and graphite. Energy Fuels **2006,** 20(1), 187-194.

(59) Zhong, J.; Song, L.; Yan, D.; Wu, Z.; Wang, C.; Xie, S.; Qian, H., A XANES characterization of structural defects in single-walled carbon nanotubes. Radiat. Phys. Chem. **2006,** 75(11), 1861-1865.

(60) Hammes, K.; Smernik, R. J.; Skjemstad, J. O.; Schmidt, M. W. I., Characterisation and evaluation of reference materials for black carbon analysis using elemental composition, colour, BET surface area and C-13 NMR spectroscopy. Appl. Geochem. **2008,** 23(8), 2113-2122.